Transactions on Engineering and Computing Sciences - Vol. 11, No. 4
Publication Date: August 25, 2023
DOI:10.14738/tecs.114.15332.
Neelakanta, P., & De Groff, D. (2023). Fuzzy Cognitron: An Unsupervised Deep-learning ANN to Identify Local Features in Medical Images via Binary Image Correlation. Transactions on Engineering and Computing Sciences, 11(4). 72-94.



Fuzzy Cognitron: An Unsupervised Deep-learning ANN to Identify Local Features in Medical Images via Binary Image Correlation

Perambur Neelakanta
Department of Electrical Engineering & Computer Science,
Florida Atlantic University, Boca Raton, Fl 33431, United States

Dolores De Groff
Department of Electrical Engineering & Computer Science,
Florida Atlantic University, Boca Raton, Fl 33431, United States

ABSTRACT

A fuzzy cognitron (FC) is proposed to model the big-data framework of deep learning (DL) conceived as a neuromorphic feedforward architecture. Pertinent concept is applied towards uncovering and predicting a labeled set of fuzzy/distorted features present locally in the gross landscape of unlabeled image space. That is, the feature data of images is assumed to exist as comingled sets of clear image space (dubbed as unlabeled details) and fuzzy/distorted image subspaces designated as labeled sections. Relevantly, the underlying learning and prediction endeavors of the test FC refer to processing the gross image features and predict subspaces of relevant labeled data having imprecise boundaries and inherent uncertainty arising from heterogeneous sources. In general, conventional artificial neural networks (ANNs) may not be compatible in elucidating the selective details of such labeled information of the test images with variety in features and posing incompleteness/sparsity of associated information. The underlying big data framework of information domains possessing fuzzy/distorted boundaries are hard to be classified with traditional ANN with veracity or conformity, de facto. Pertinent to such big data ambient of vague details and gray truth, complex computational schemes and methods are largely sparse in the existing literature. As such, conceived here is a novel class of deep ANN approach based on robust fuzzy models towards addressing the aforesaid data-possessing. Hence, the test FC is proposed with an architecture, which conforms to a modified crisp version of cognitron originally due to Fukushima. The associated neural computation is devised to handle the test (analog) image depicted in a binary matrix format; and, a binary image correlation algorithm is pursued to establish the local features of the labeled subspace in the image. A simulation example is presented towards medical image classifications and the operation and efficacy of the proposed FC are outlined. Relevant results are presented and discussed.

Keywords: Fuzzy deep ANN, Fuzzy cognitron, Fuzzy Langevin-Neelakanta machine, medical images, Local labeled features, Global unlabeled features, Deep learning, AI, Cross-correlation

INTRODUCTION

This study is motivated to evolve a fuzzy cognitron (FC) that depicts the architecture of a deep artificial neural network (deep ANN) designed to assess the details of imprecise image subspaces having overlapping fuzzy/distorted regions. The underlying concept refers to neuroscience theoretics extended to apply deep learning (DL) concepts in uncovering and predicting fuzzy/distorted features in a test image. The images considered thereof (such as, those of interest in clinical contexts) typically bear information, which depicts the complexity of a big data ambient; further, inasmuch as such images may include fuzzy/distorted subspaces, unique models towards learning and prediction efforts of the test FC are considered, based on fuzzy rules applied in fragmentizing and classifying subtle details with associated dissonance.

In order to achieve accurate and adjusted insights in predicting desired image details, relevant approach of DL focused here simulates the contexts of artificial intelligence (AI) in learning and prediction processes on the big-data framework of the image space *via* a deep ANN architecture framed as the proposed test FC. The overall space of the image is segmented thereof into two classes: (i) Subspaces with identifiable distorted/fuzzy features identified as labeled region; and, (ii) the general landscape of the image considered as an unlabeled space with no distortions/fuzzy sections.

To implement the objective of the study towards precisely assessing the said image features, the analog test image is first represented as a two-dimensional (2D) feature map of digitized pixels. That is, the test image is mapped as a 2D matrix of pixels with each pixel assigned a score value as decided by the associated image features. The pixel scores are determined *via* a compatible algorithmic suite of binary correlation of details pertinent to the test image *versus* those of a reference template pixel matrix. The pixel scores are then used as the input data at the deep ANN where the required neural computations are simulated consistent with the paradigm of DL. The proposed deep ANN of FC consists of a multiple set of paired layers having interconnected set of neuronal units organized as a feedforward architecture; and, self-organization of the entire FC is rendered with unsupervised learning (USL) schedule exercised in each of the paired layers independently. The associated deep ANN computations performed on the input data involves achieving self-organization of the net by two steps: (i) Implementing a learning/training phase, which refers to a repetitive presentation of several stimulus/excitatory patterns (of the image) addressed as inputs of the test FC; and, a feed forward schedule is pursued to train each subdomain of the paired layers across the network. (ii) Performing the prediction phase wherein a fresh set of stimulus/input data representing the test image is addressed at the input of the trained FC and corresponding details on the segregated subdomains of labeled image pattern is availed as the eventual result at the output layer.

The performance of the conceived test FC is further augmented with the following inclusions: (a) Considerations of fuzzy Langevin-Neelakanta machine [1] are adopted in the USL loop towards realizing a squashed output, which in turn generates iteratively a weight correction coefficient applied to the interconnections across the neuronal units in each paired-layers towards an assured self-organized convergence to a global minimum. (b) Pertinent, changing of interconnection weights exercised in the USL loop involves using a learning coefficient (α) obtained *via* a Hessian matrix algorithm prescribed at the neural network input; and, this

learning coefficient enables fast convergence as described in [1][2]. Lastly, inasmuch as the input details of the test FC consist of global image features (marked as unlabeled information) plus randomly diffused fuzzy/distorted details (indicated as labeled items), the underlying analyses involve specific efforts to identify and segregate the labeled and unlabeled entities; eventually, the output of the deep ANN is rendered as defuzzified information *vis-à-vis* the required labeled image features. In all, the fuzzy input/output response of the proposed neural complex conforms to a meaningful representation of a neuromorphic structure facilitating fuzzy-input *versus* defuzzified output details.

The paper is organized as follows: Commensurate with the general considerations on AI and DL, the motivational efforts exercised on the deep ANN architecture (conceived as proposed FC) are described in the (present) introduction. In the pursuing section, medical images and the associated fuzzy/distorted heuristics are outlined and the application potential of the proposed FC is indicated towards identifying locally-specified, labeled subspaces exhibiting distorted and/or fuzzy features in test medical images [3][4]. Hence an annotative note on the test deep ANN with a descriptive narration on the operational details of the network conceived as the proposed FC with the associated heuristics of architecture details is presented. In essence, as stated before, pertinent deep ANN algorithm presorts/encodes labeled details of distorted/fuzzy locales diffused across unlabeled domains of the test image. Relevant exercises of input-output transformation in the FC conform to yield decoded output on labeled features discriminatively. Descriptions of learning and prediction phases implemented on the test FC are presented in the pursuant section; and, deduced results relevant to an exemplar of medical image are posted subsequently. Discussions on the results and concluding remarks are presented in the last section of the paper.

MEDICAL IMAGES AND ASSOCIATED FUZZY HEURISTICS

The medical images acquired in clinical contexts can be viewed as a conglomeration of a huge collection of pixels proportionate to the extent of sharpness *vis-à-vis* finer structural details of the image. That is, such image spaces can have regions of clarity with crisply observable sections; as well as, there could be subdomains having imprecise boundaries with overlapping pixel data of distorted/fuzzy details. The application potential of the proposed FC refers to identifying pertinent local subspaces (exhibiting distorted and/or fuzzy features). A deep ANN algorithm pursued thereof presorts/encodes the labeled details of those distorted/fuzzy locales diffused across unlabeled domains of normal image features.

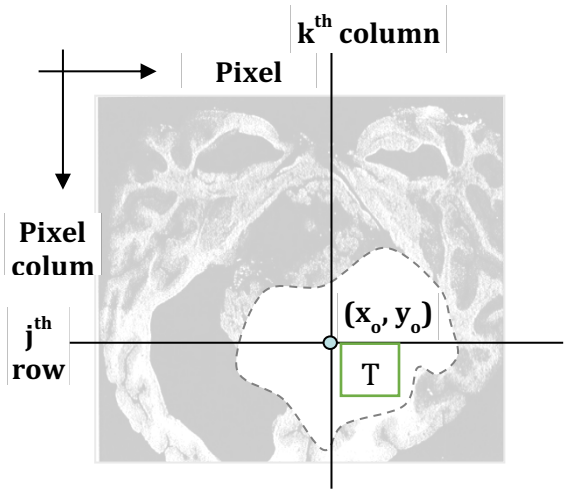


Figure 1: A hypothetical image-space of unlabeled region with a distorted/fuzzy (labeled) subspace, identified as, T.

Shown in Figure 1, for example, is a hypothetical image-space globally depicting an unlabeled background plus a "distorted" region (**T**) constituted by a fuzzy/distorted cluster of details having a centroid at (x_o, y_o). The deep ANN analyses pursued refer to performing necessary input-output transformation in the test FC using relevant algorithmic suites aimed at obtaining discriminatively a decoded output on local features of the labeled subspace, **T** (for example, corresponding to certain pathological region).

Further, the associated data of labeled, fuzzy/distorted sections of the image could refer to overlapping details of vagueness and infestation of sparse contents with imprecise contours of transitions. As such, the image space in question would represent a complex framework of information consistent with big data ambient with explicit dissonance observed while fragmentizing and classifying the underlying details; and, in order to analyze and classify such subdomains, it would require unique models based on fuzzy rules.

Thus, images of clinical interests, in general would require modeling the associated space specified as two subsets of fragmented details: (i) Data sets possessing information that are mostly sparse having small disjuncts. They represent the said *labeled items, mostly* existing in low proportions with fuzzy and/or distorted characterizations; and, (ii) a larger content of image details that are crisp and proportionately extensive coexist. It is identified as unlabeled information. In Figure 1, the unlabeled region provides a background for the "distorted" region constituted by a fuzzy/distorted cluster of details having a centroid at (x_o, y_o) depicting the labeled subspace as indicated above.

This distorted subspace with possible overlapping details of vagueness and infestation of sparse contents having imprecise contours of transitions can be regarded as being a "noisy" region. In contrast, rest of undistorted/crisp sections denote unlabeled background possessing clarity of image details; and, such unlabeled sections can be considered as a reference background conforming to distortion-free, information-bearing set of "signal" counterparts of the image. Relevantly, the extent of distortion and fuzziness in the labeled image subspace can be implicitly specified by a parameter akin to signal-to-noise ratio (SNR) of communication

theory [5]. In other words, the distorted/fuzzy image space can be construed as a "noise-limited entity" and marked with a "label" in terms of aforesaid SNR values. Inasmuch as the labeled regions lack clarity of image details (and, possibly having overlapping subsections with fuzzy boundaries of separation), they depict uncertain features or sparse information characterized by posentropy heuristics (in Shannon's sense). In contrast, the coexisting unlabeled section represents a clear set of pixel arrangements with tractable crisp transitions showing negentropic characteristics.

For analysis purposes, the analog test image is first converted into a pixel space as mentioned before and viewed in terms of the associated pixel-by-pixel details as follows: The entire image space is divided into orthogonal sets of discretized pixel rows and pixel columns. Resulting binary matrix [$\mathbf{m} \times \mathbf{n}$] of the image is thus, constituted by a set of **m**-rows and **n**-columns; and, each pixel location corresponds to the intersection of a row (or a horizontal sequence of pixels) and a column (or a vertical sequence of pixel); and, each location of intersection of rows and columns is indexed respectively by the sets, j = (0, 1, 2, …, m) and k = (0, 1, 2, …, n). Binary values {1, 0} are then assigned for each pixel elements on the basis of relative gray-level status in the analog image. Thus, the matrix space of pixels generated would denote randomly disposed binary values, 0's and 1's mapping equivalently the analog test image.

Relevant to the labeled, "noisy" subsections of the image, the proportionate extent of "corruption" or "image-distortion" (relative to reference/undistorted image space of unlabeled sections) can be estimated in the vicinity of a given cluster of labeled pixel sites centered at, (x_o, y_o) (depicting the intersection coordinate of j^{th} row and k^{th} column). This focused region refers to the distorted/fuzzy locale in the image and is statistically constrained with a probability of error associated with the random values of the set of pixel values (1 or 0) estimated around (x_o, y_o). Thus, in Figure 1 considering the noise-free, uncorrupted site in the image space of unlabeled region, relevant image-information (negentropy) details can be denoted as I_o bits (in Shannon sense). And the labeled region indicated as the distorted subspace of the image, corresponds to posentropy aspects of information, which can be written as ($I_o - \Delta I$) bits, where ($-\Delta I$) implies the decreased value of I_o resulting from noisy, spatial-jitter or fuzzy attributes due to distortions present in the labeled subspace. Hence, a measure/metric of (relative) statistical divergence [6] [7] of I_o *versus* ($I_o - \Delta I$) (or *vice versa*) can be assumed to prevail at or around (x_o, y_o). In essence, DI represent a jitter variable, when superimposed on uncorrupted "signal", $\bar{S}$ (x_o, y_o) at the location (x_o, y_o) would correspond to a relative measure of distorted features in the test image. Relevantly, the expected root-mean-squared (rms) jitter can be expressed by a "noise" related function, $J_r(x_o, y_o)$ pertinent to the labeled test-image *versus* the "signal" term of unlabeled, uncorrupted image space. The signal-to-noise ratio (SNR) concept of communication theory [5] can be applied in image comparison suites (of labeled and unlabeled subspaces) corresponding to the average pixel area of the image subspace located at (x_o, y_o); and, a relevant "spatial SNR" (SSNR) can be defined as follows: SSNR = $(\bar{S})^2 / J_r^2$. In this context, the SSNR implicitly specifies the probability of "erroneous" pixel data or posentropy features that implicate the image integrity at or around (x_o, y_o) within the specified blurring limits of the jitter in the image-space [8] [9].

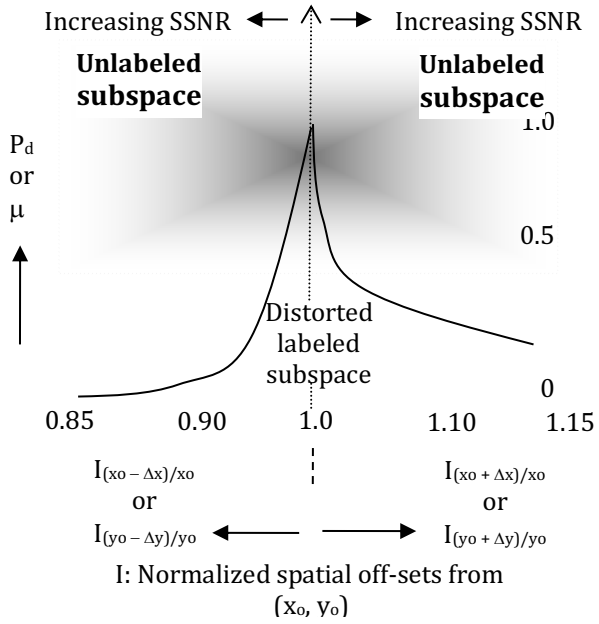


Figure 2: Probability (P_d) or membership function (m) depicting the extent of distortion/fuzziness *versus* $I_{(xo \pm \Delta x)/xo}$ or $I_{(yo \pm \Delta y)/yo}$ ascertained with reference to the locale (x_o, y_o)

Considering the unlabeled subspace as a pre-annotated reference, the relative aspect of labeled region, one can specify a probability value for the pixels in the image-distortion subspace, as $P_d|_{(i = 0, 1, 2, ..., m)}$; and, it implies the probability of distorted information value (*versus* corresponding undistorted information probability) of the unlabeled region. The value of P_d is implicitly dependent on SSNR parameter indicated above. Explicit expression for P_d is available in [8]; and, in Figure 2, P_d is plotted as a function of $I_{(xo \pm \Delta x)/xo}$ or $I_{(yo \pm \Delta y)/yo}$ with reference to the locale (x_o, y_o), where the distortion-prone region is taken as of width Δx and height, Δy. Further, the probability value, $(0 \leq P_d \leq 1)$ concurrently depicts a membership grade, $(0 \leq \mu \leq 1)$ of the associated fuzzy variations. Note the asymmetry of probability or membership grade values in Figure 2 along $(x_o - \Delta x)/x_o$ or $(y_o - \Delta y)/y_o$ and corresponding $(x_o + \Delta x)/x_o$ or $(y_o + \Delta y)/y_o$ directions. The reason is that the statistics of distortion variables need not be symmetric around (x_o, y_o).

In essence, the distortion-prone region in the image depicts a subspace of corruptions assumed to smear across the location of (x_o, y_o). It imposes thereof an imprecision on image integrity information; relevantly, one can specify a probability value of image-distortion for the i^{th}-subspace in the test-image, $P_d|_{(i = 0, 1, 2, ..., m)}$. The generic description of P_d in this subspace also specifies an attribute of vagueness *vis-à-vis* the pixel-position variables, at (x_o, y_o) implying the distorted image being described as being fuzzy. Relevant membership value would specify its relative belongingness to ideal (reference) image subspace or distorted test-image subspace.

In all, the image data (of Figure1) subjected to analysis (*via* neural network, or otherwise) could perceivably possess fuzzy attributes as well as, stochastic features *vis-à-vis* diverse mix of labeled and unlabeled constituents. In practice, the fuzzy details mapped in terms of a membership function, translate the underlying linguistic aspects of fuzzy, overlapping

subspaces labeled and unlabeled segments into relatively quantifiable measure. The underlying fuzzy details can be regarded as an "error'' feature of indistinguishability across overlapping subspaces. That is, inasmuch as the location of transition of the segments is not distinct, the fuzzy transition may be identified to follow certain rules; however, such fuzzy transitions may not reasonably (and robustly) show the precise site of true transition. Hence, any fuzzy transitional domain can be regarded as a region of "spatial jitter" with a characteristic parameter defined earlier as SSNR; and, relevant diverse features in the labeled and unlabeled fuzzy spaces are (assumed to be) statistically independent [8-11]. Corresponding to the fuzzy subspace under discussion, the defuzzified value of the underlying fuzzy variable at the centroid coordinate (x_o, y_o) is decided by upper- and lower-bound profiles of the m-value. Pertinent details on defuzzification process can be found in: [6][8-11].

In the present efforts concerning deep ANN, the associated data set of the test image space is regarded as a fusion of large amounts unlabeled data plus some extent of labeled region of 'pertinent', distorted/fuzzy subspace as mentioned before; and, relevant DL models rely on learning the basis of differentiating subtle variations in the data elements of labeled and unlabeled details. In essence, the learning and prediction schedules of ANN refer to classification of a data set with skewed class proportions of labeled and unlabeled details posing a *class imbalance* problem. The unlabeled classes that make up the test image here, refer to a large proportion of data set (of majority classes) and the labeled details make up a smaller proportion of minority classes. This imposes a meta-tagged, constrained knowledge in training and prediction phases of the ANN, specific to snippets of unlabeled and labeled contents of mixed details. This is warranted because, a few iterations at the commencement of annealing or iterative corrections performed (in building the predictive model being sought) across the stretch of deep architecture of multiple layers should lead to tangible guesses on the pertinence of the data being handled *versus* the contents of the output being predicted. This would prevent the annealing exercise getting trapped at a local minimum instead of reaching the global minimum at the goal-seeking terminal phase and achieving a faster convergence [6][7].

Suppose a specific subspace of the test image is fuzzy/distorted, relevant digitized cells of the matrix denote overlapping regions with imprecise boundaries; and, the associated fuzzy information considerations can be viewed in terms of the heuristics of fuzzy theoretics. Relevant rule-based algorithms typically use fuzzy partition using equally distributed triangular membership functions and exercise a fuzzy rule-base in segmenting each class [12]. Present study implies uncovering and discriminatively predicting overlapping features of such fuzzy images *via* a set of 2D fuzzy binary pattern of pixels that map equivalently the underlying analog details; that is, relevant "… algorithm looking at an image simply sees rows of pixels…" [13].

Evolving and implementing discriminative algorithms towards elucidating local features of fuzzy/distorted images (rendered as a subdomain of sparsely prevalent labeled data set of 2D binary pattern of pixels) coexisting in a larger domain of (unlabeled) sharp-image details refer to computational steps addressing the underlying classification problems in discriminative frames. Relevant efforts form the scope of the present study. For this purpose, as outlined before the 2D-pattern of the test analog image cast into digitized (binary) matrix format is subjected to computational steps towards estimating a binary-correlation score (*via*

compatible algorithm) between the digitized bit-map of the test-image *versus* a reference template of 2D binary pattern as illustrated in Figure 3. The computed correlation score of any pixel enables ascertaining the discriminating features of the test image at that pixel space. The details of Figure 3 are as follows:

When the analog image details (such as in Figure 1) are represented as a framework of 2D-set of pixels mentioned earlier, the computational steps towards predicting the pattern of labeled knowledge sought as the outcome involve establishing a 2D binary-correlation between the digitized bit-map of the test-image *versus* a template of 2D binary pattern as shown in the flow chart of Figure 3. That is**,** pattern comparison between a test image *versus* a template involves recognizing the underlying pixel characters in terms of spatially-discretized set of binary intensities [3][4].

The computational steps towards estimating the 2D binary-correlation score between the compared sets of binary matrices (Figure 3) are as follows:

- The analog test-image is first converted into a matrix of [**m** × **n**] binary intensity array representing a 2D-set of binary characters. Each row corresponds to a [**1** × **n**] state-vector and likewise, each column denotes a [**m** × **1**] state-vector.
- The template image pattern, (also of [**m** × **n**] array size) is filled with all its array elements as binary representations of 1. The template is used as a reference for pixel-by-pixel comparison.
- That is, the binary entry in each pixel of a row (say, j^{th} row) of the test image is compared against corresponding pixel entry of the j^{th} row in the template *via* a compatible algorithm; hence, the resulting correlation score is determined; and this procedure is repeated for the entire set of rows.
- The above step of binary comparison and evaluating the correlation scores is also repeated for all the pixels column-wise across the entire image matrix.
- Compatible 2D-comparison algorithms can be used towards estimating the binary image correlation score as above. Various algorithmic suites are available in deciding such correlation scores as listed later. Relevant algorithms address two avenues of scores of pixels pertinent to row-to-row and column-to-column comparisons.

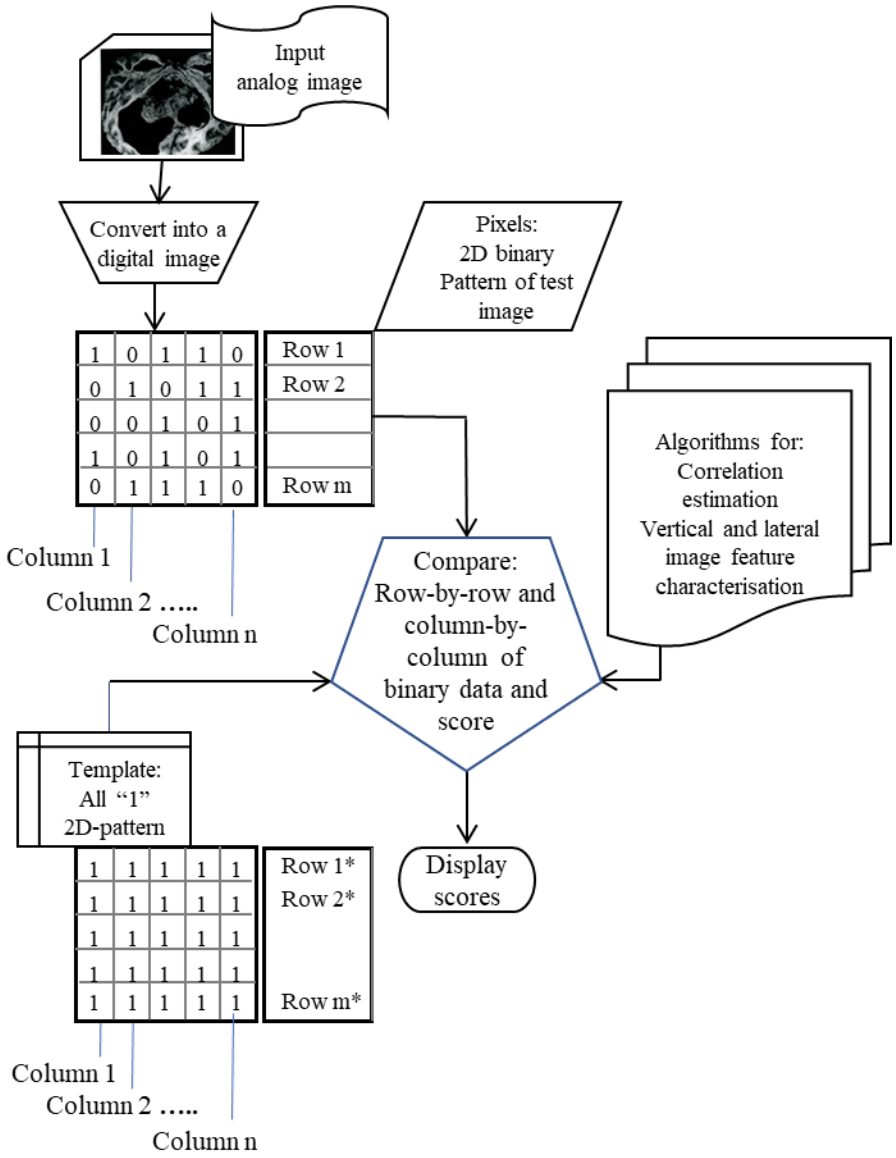


Figure 3: A flowchart on computational steps towards estimating 2D binary-correlation score (*via* compatible algorithm) between digitized bit-map of the test-image *versus* a template of 2D binary pattern

A DESCRIPTIVE NOTE ON PROPOSED FC

With reference to image analyses, a big data constraint may exist in precisely specifying the image details *vis-a-vis* enormous datasets implied in training and prediction phases of the test ANN adopted towards deciding image features. In the past, a class of compatible ANN architectures with required capabilities have been conceived [14] as hierarchical convolutional neural networks (CNNs) and they mostly denote *ad hoc* versions of multilayer perceptron where, the CNN does feed-forward and/or recurrent information processing over time through a set of multiple layers (with each neuron in one layer massively interconnected to all neurons in the next layer) so as to yield the required results as outputs by detecting and segmenting subtle details of the input.

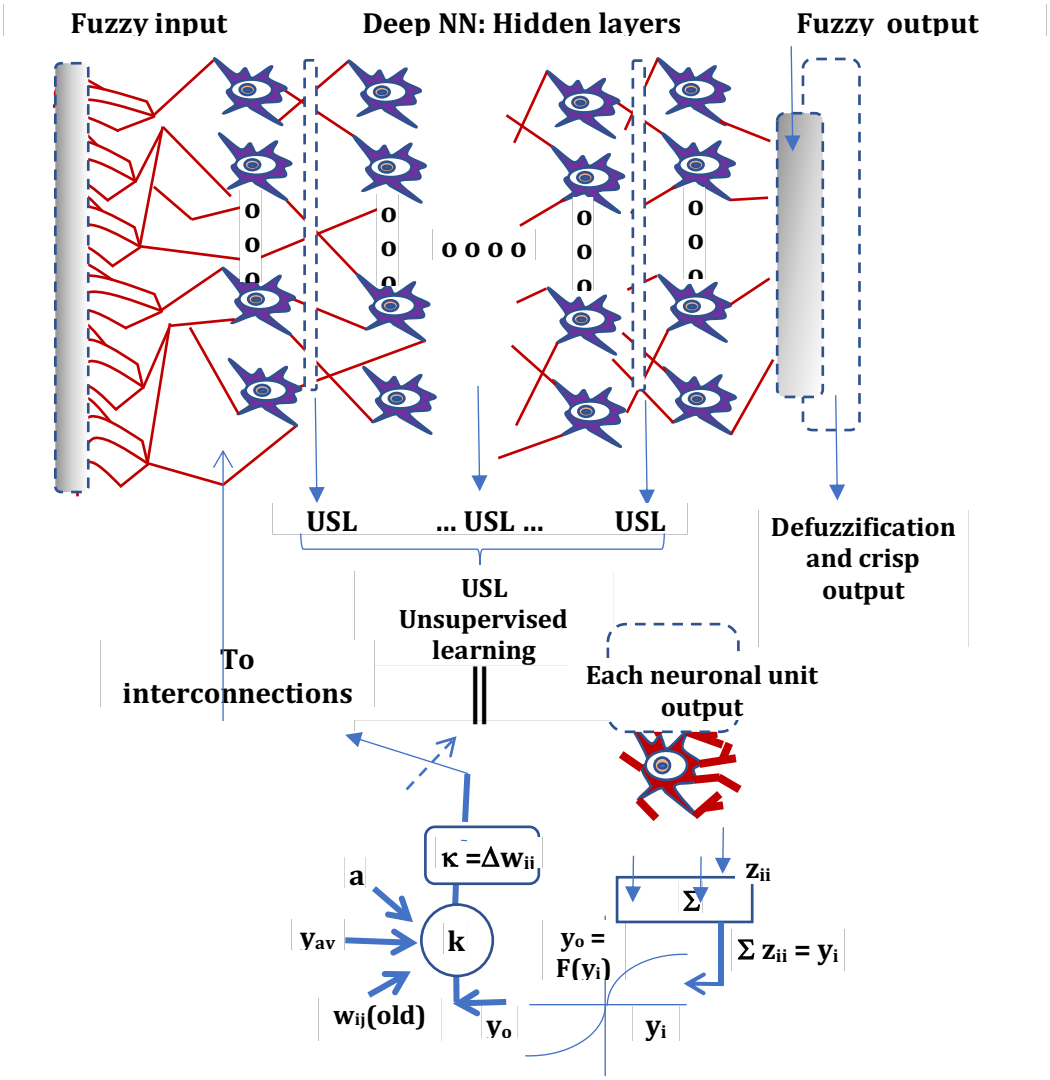


Figure 4: Proposed fuzzy cognitron architecture for deep ANN simulation

(z_{ii}: Output from each neuronal unit of a paired (i, i)th layer and $\Sigma z_{ii} = y_i$: Summed value; F(.): Squashing sigmoidal function and $y_o = F(y_i)$; w_{ij}: Weight of each interconnection; y_{ave} = Mean value of y_i taken as a reference base; α: Learning coefficient; κ: Function of (w_{ij}, y_{ave} and α) depicting weight modification value, Δw_{ij} applied on interconnections)

There are two categories of fuzzy-neural networks generally adopted in practice as detailed in [6]. The first group of neural networks uses a set of fuzzy weights in the network for fuzzy reasoning. For example, fuzzy neural networks have been evolved with fuzzy signals processed by fuzzy weights and biases and relevant "if-then" rule-based learning characteristics. Another category of fuzzy neural networks involves input data that are fuzzified at the first or the second layer, but the network weights themselves may not be fuzzy. A typical version thereof is based on the concept of "fuzzy curves" to identify the significant input variables, estimate the number of rules needed in the fuzzy model and determine the initial weights for the neural network. The fuzzy curve is generated *via* centroid defuzzification for each input variable.

The architectural details and functional aspects of the proposed FC (illustrated in Figure 4) are as follows: The test architecture of deep ANN is made of a cascaded set of paired-layers, (L_1, L_2), (L_3, L_4), …, (L_r, L_s), …, (L_t, L_{t+1}), where the last pair of t^{th} and $(t + 1)^{th}$ layers depict the output unit.

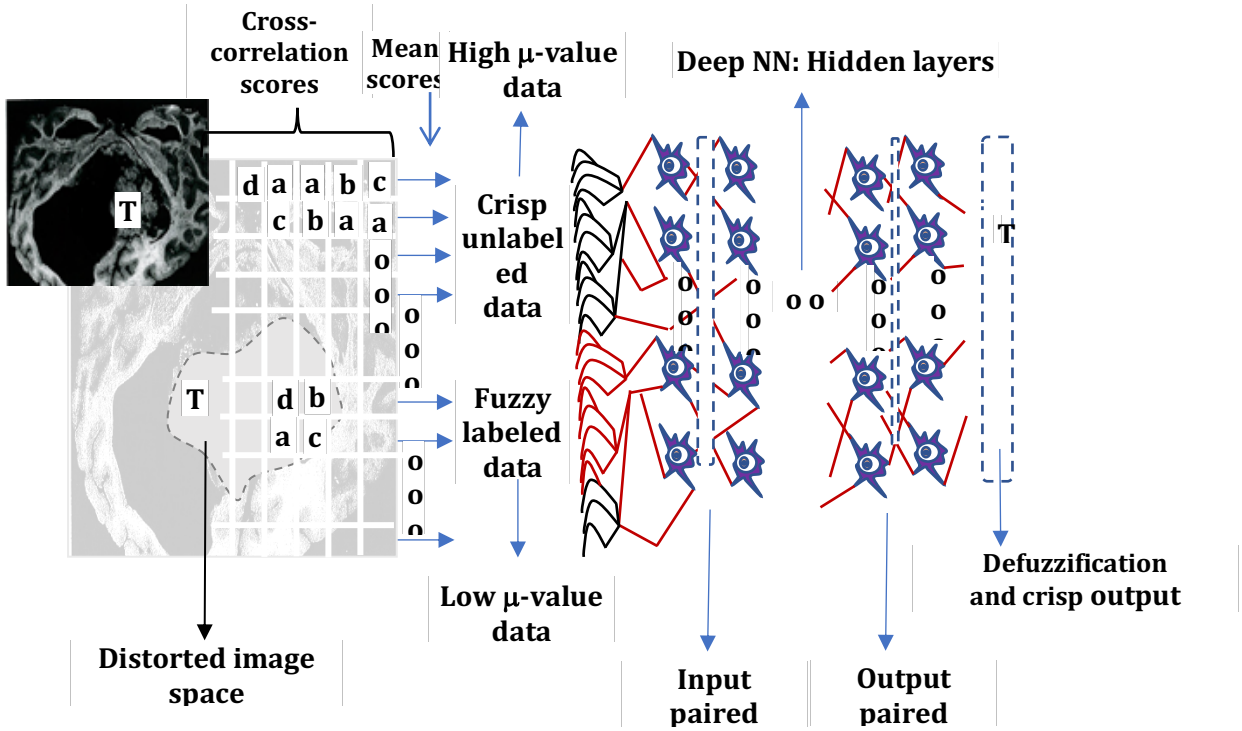


Figure 5: Deep ANN processing comingled sets of crisp/unlabeled and fuzzy/labeled data inputs: The pixel matrix of the test image contains normalized values of 2D binary-correlation hypothetical scores represented by the set {a, b, c, d, ….,} that are applied as ANN inputs.

An augmented deep ANN pursuit proposed here refers to the feasibility of including fuzzy/distorted attributes as well in the data being processed; and, a relevant architecture conforms to a fuzzy cognitron designed with an input layer supporting an extensive number of input neurons each receiving the binary details (correlation scores) from the 2D matrix of the test image; and, the 2D-matrix is presumed to contain comingled sets of unlabeled (distortion-free) features plus labeled features of fuzzy/distorted information in the test image. Further, the test deep ANN has a multiple set of cascaded pairs of hidden layers; and, as stated earlier, each pair is independently trained *via* unsupervised learning (USL) towards self-organization. The architecture of using such cascaded set of individualized paired set of layers is akin to that of Fukushima's cognitron [15][16]; but, it is modified to match the motivated context of present study towards including fuzzy data classification. Simulation results presented thereof should establish a desirable efficacy of the proposed concept; and, relevant algorithmic suites pursued should enable fast and assured convergence with uniquely specified learning rate as well as, facilitate achieving better (more accurate) results on predictions. Further, the underlying information processing is perceived to include the so-called Langevin-Neelakanta machine concept [1] with the associated adjustable squashing function adopted in the USL loops.

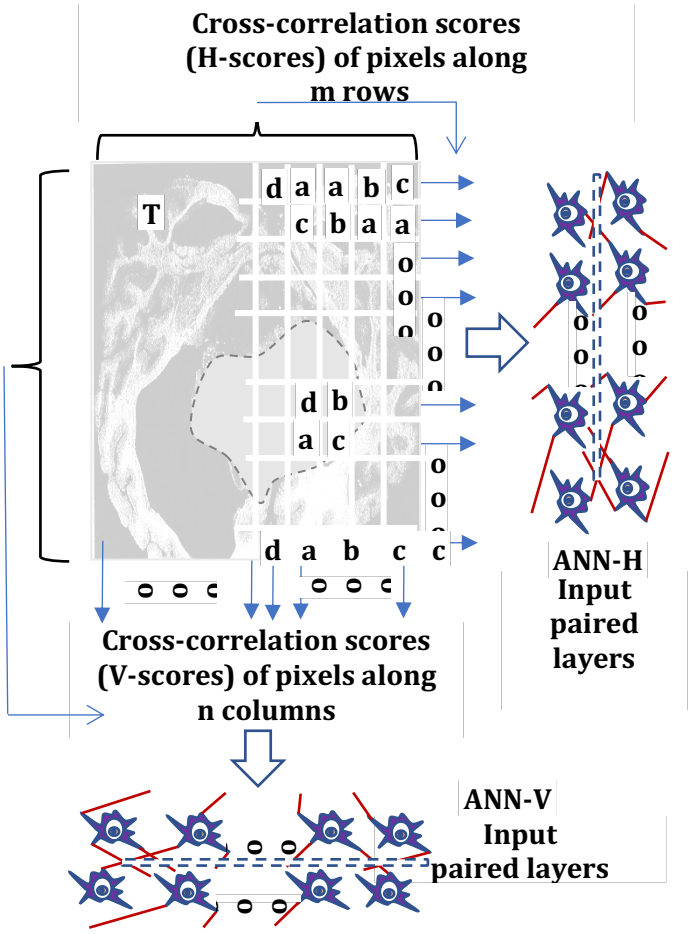


Figure 6: Collected sets of normalized values of 2D binary-correlation scores of the test image applied at the inputs of two parallelly-operating, independent deep architectures: ANN-H and ANN-V that process the inputs of H- and V-scores respectively

Further, the proposed FC uses two parallelly-operating, identical architectures of deep ANNs shown in Figure 4. They are identified here as ANN-H and ANN-V accommodating two sets of scores, namely, H- and V-scores. The cross-correlation scores of pixels along m rows of the pixel matrix denote row-by-row pixel details and they are indicated as H-scores used as inputs of ANN-H for computations; and, the cross-correlation scores of pixels along n columns of the pixel matrix depict V-scores of column-by-column pixel details used as inputs of ANN-V for processing. The ANN inputs as above correspond to mean values of the normalized H- or V-scores in each row or column respectively).

Deep ANN processing of comingled sets of crisp/unlabeled and fuzzy/labeled data inputs in the test FC is illustrated in Figure 5 where the pixel matrix of the test image contains normalized values of 2D binary-correlation hypothetical scores represented by the set {a, b, c, d, ...,} that are applied as ANN inputs. Accommodation both H- and V-scores in the ANN-H and ANN-V of the test FC is further illustrated in Figure 6.

The schedule of unsupervised learning (USL) in Figure 4 is exercised at each paired-layers as indicated. Considering the expanded illustration of USL in Figure 4, the collective outputs (say, P_{ij}), of neuronal units of any paired-layer, lead to a corresponding summed output (y_{in}) and it is subsequently squashed by a sigmoidal function, $F(y_{in})$ [7]. Relevant squashed output, $y_o = F(y_{in})$ is then multiplied by a scaling function, which functionally alters y_o to yield a weight modification value, $\kappa = \Delta w_{ij}$. This weight modification is iteratively applied to adjust the existing interconnecting weights, w_{ij} between the paired layers until convergence towards minimizing, y_{in} is achieved. The scaling function indicated is decided by: (i) y_{ave} depicting the mean value of y_i taken as a reference steady-state value of the underlying dynamics; (ii) α, denoting the learning coefficient; and, w_{ij} as mentioned above, is the present weight of interconnections. Conventionally, a simple hyperbolic tangent (sigmoidal) function [7] is used as the squashing function, F(.) in ANN simulations; however, in the present study, the sigmoidal function chosen conforms to the heuristics of the so-called Langevin-Neelakanta machine as described [1].

In all, the *tasks* in *deep neural networking* objectively imply processing a set of raw input data so as to extract required features or the desired/labeled data from it. The extracted details are based on the inherent capability of classification in an arbitrary input-output mapping and specify a predictive classification of the desired data at the output. That is, the ANN is trained to classify the labeled and unlabeled data supplied as the input and spot the labeled pattern as predictive output. Relevant training and prediction schemes in the proposed deep ANN simulation is based on unsupervised learning (USL) method indicated in Figures 4 and 5.

TRAINING AND PREDICTION PHASES PLUS DEFUZZIFICATION

The proposed fuzzy cognitron of Figure 4 illustrates how the input data is processed iteratively towards self-organizing the interconnected neuronal units contained in each paired layer and eventually yielding the desired results at the output layer. The output is then subjected to defuzzification to provide crisp details. The functioning of the proposed FC is demonstrated here with necessary simulations. Relevant steps involved are outlined as follows:

1. As indicated earlier, the conceived test FC consists of a cascaded set of paired-layers, (L_1, L_2), (L_3, L_4), …, (L_r, L_s), …, (L_K, L_{K+1}), where the last pair of K^{th} and $(K + 1)^{th}$ layers depict the output unit. In the present study, the test FC (of Figure 4) adopted for simulation has three pairs with K = 3 with unsupervised learning (USL) administered on each pair. That is, the structure of Figure 4 is constructed with a total of 6 layers: One pair of input layers, one pair of output layers and one pair of hidden layers. Further, each layer is presumed to have 7 neuronal units in each of 6 layers (paired into 3 pairs); and, each pair is represented in the simulations as: P_1: $L_1 \leftrightarrow L_2$; P_2: $L_3 \leftrightarrow L_4$ and P_3: $L_5 \leftrightarrow L_6$. The associated simulation/operational details of the test cognitron (used in the analysis of an exemplar medical image) are as follows:
2. Suppose a hypothetical test image is as shown in Figure 1 having a fuzzy, distorted subspace (**T**). The analog image is first converted/digitized into a matrix format of pixels as follows: Given an image in 2D analog format, it is first changed into a gray-scale image and then into a binary version [3][4] of **[m × n]** array of bits depicting the image being processed. That is, the test image is transformed into a column vector representation by stacking up the consecutive rows of each image as an **[m × n]** array. In the binary format, the white pixels are assumed as "1" and dark pixels are taken as "0". (Further, in constructing the binary array, the analog test image is initially sized (cropped) and

"framed" into a rectangle/square prior to its conversion into a binary format. This would confirm the matrix-size of the image being compatible in size for computations). Also, another analog image is concurrently framed as a reference template of **[m × n]** of 2D binary array with all its pixels depicted by the binary digit "1" as shown in Figure 3, where this reference template has all its matrix elements (pixel values) taken as, 1. This template is framed in order to evaluate the extent of pixel features (of gray levels) in the matrix-formatted test image (relative to the pixel data in the template).

3. The first layer, L_1 paired with L_2 of Figure 4 receives the input data, which conforms to a randomly comingled set of labeled, fuzzy/distorted image details and unlabeled information of non-fuzzy/distorted sections of the test image. The addressed inputs progress ahead across interconnected neurons at the pair L_1 and L_2 (marked as P_{ij}, i = 1 and j = 2) and subsequently routed along the entire sets of paired layers through the massive interconnections.
4. The USL is exercised on each of the three pairs. That is, at each paired layer, the prescribed USL is implemented as follows: Relevant outputs of each paired layer are then summed to yield, y_{in} as shown (Figure 4), which is then squashed by a sigmoidal function, F(.) so as to get a limited output, $y_o = F(y_{in})$. It is further modified appropriately with a function κ decided by a learning coefficient (α), present value of interconnecting weights, w_{ij} (across each of paired layers of the set {L_r and L_s}) and the mean value (y_{ave}) of y_o. The resulting value of κ is the weight modification/adjustment coefficient ($\pm \Delta w_{ij}$) applied on the interconnections. The adjustment is performed for iteration exercised with each input data until, convergence is achieved, as observed with a minimized value of y_{in}.
5. The learning coefficient (α) used in the simulations is determined as follows: As mentioned earlier, in the test deep ANN, each layer is conceived to hold seven neuronal units in each of 6 (or three paired) layers; and, each pair the test simulation conforms to a set of the input data {$\mathbf{x_1, x_2, ..., x_7}$} addressed at the input pair of layers, (L_1 and L_2). In the simulations performed, relevant input data set {$\mathbf{x_1, x_2, ..., x_7}$} consists of normalized values of seven observed details of the test image expressed in terms of cross-correlation entries of H- or V-scores in the pixel matrix. For the given input set, a corresponding transpose $[\mathbf{x_1}, \mathbf{x_2}, ..., \mathbf{x_7}]^T$ is then simulated and hence, a relevant **[7 × 7]** Hessian matrix [**HD**] = $\mathbf{[x_1, x_2, ..., x_7]^T . [x_1, x_2, ..., x_7]}$ is deduced. It refers to a symmetric square **[7 × 7]** matrix yielding one non-vanishing eigenvalue as a diagonal element. That is, for a given ensemble of input data set there is one non-vanishing eigenvalue is obtained and the procedure to deduce the value of learning coefficient (α) using the aforesaid [**HD**] is described in [2].
6. Several inputs (each with labeled plus unlabeled data) are successively addressed as training patterns constituting the training phase. Given one set of data, such multiple sets of input data can be obtained as pseudo-replicates *via* bootstrapping shuffling [17]. For each set of input data, the training/learning phase is as follows: Reference to layers L_1 and L_2, the converged output (realized *via* USL-based self-organization) at the associated neuron set {$n_1, n_2, ..., (N = n_7)$} of L_2 is transferred/fed-forward as input to the neurons in the subsequent layer L_3 of the consequent paired-layers where, USL is again applied and so on until training the final pair of layers, L_5 and L_6 is completed as above (monitored as minimized/converged value of y_{in}).

7. With the training phase completed along the cascaded pairs as above, the converged set of details on weights $\{w_{ij}\}$ at each pair (L_r, L_s) and the converged neuronal states, $\{z_1, z_2, \ldots, z_n, \ldots, z_N\}$ on N (= 7) neurons of each layers are kept frozen (stored) for use in the subsequent prediction phase.
8. Simulation of prediction phase on the test cognitron is as follows: A fresh test data set $\{\psi_1, \psi_2, \ldots, \psi_{N=7}\}$ containing unlabeled and labeled entities is addressed at the input layer L_1 towards prediction of the required labeled information coexisting with unlabeled details. That is, this fresh data set is an exemplar intended for the prediction of its labeled content. The network processes this test data with the frozen sets of weights: $\{w_{12}\}$, $\{w_{34}\}$, $\{w_{56}\}$ obtained from the completed training phase in the feed-forward exercise.
9. The ways of obtaining cross-correlation scores by comparing the pixel arrays of the test image and the template are outlined in the next section.
10. The output obtained in the prediction phase refers to the mix of labeled and unlabeled features of the test image, with the labeled (desired) feature data emphasized, by virtue of its membership values decided in the defuzzification procedure as outlined in [8][9].

Pursuant to simulation details as above, in the following section, simulation results obtained are presented with reference to identifying local subspaces exhibiting distorted and/or fuzzy features in a medical image. In essence, the simulation experiment pertinent to test deep ANN algorithm presorts/encodes labeled details of those distorted/fuzzy locales situated across unlabeled domains in the rest of the test image. Relevant exercises of input-output transformation in the FC conforms to yielding discriminatively, the decoded output on local features.

SIMULATION RESULTS ON THE TEST MEDICAL IMAGE

As narrated in the previous section, the simulation exercise pursued refers to a medical image having comingled sets of labeled and unlabeled details as mentioned earlier. Typically, the diagnostic aspects of medical images in a clinical setting implicitly require knowing point-by-point correspondence between sites in a reference template (of an ideal image) *versus* those in a test-image. For example, two such images may be of a single patient captured at different times, (such as during a mammography examination involving repeated imaging before and after the injection of a contrast agent etc.); and, they can be compared against each other to know the distinguishing features of any local significance. Also, relevant images can be of a single patient viewed by different imaging modalities (such as magnetic resonance imaging and computerized tomography). Such redundant imaging details are often acquired to provide complementary information for image comparison and evaluate the extent of any pathology involved. The art of comparatively viewing a localized point in one image and its corresponding point in another refers to a transformational relation often known as *medical image registration* [18]. The procedure of such image registration calls for a template-to-test image matching technique.

Essentially, the registration modeling corresponds to 2D-matching of pixel-by-pixel characteristics and it implies the following: The granular features between a template and a test-image provide singular or (microscopically local) details. In a more diffused sense, pertinent image comparison yields scores that offer cumulatively global (or macroscopically

extended) features of the image, which are prevalent as unlabeled data plus locally significant, labeled information as outlined earlier.

Recognition of variations existing between images (for classifying them) can be done in a number of ways as described for example, in the classical literature [19]. Notwithstanding the prevalence of such methods, the study addressed in this paper is conceived and motivated by the consideration of comparing locally-significant micro-, meso- or macroscopic artefacts (that signify labeled features of fuzzy and/or distorted contents) in a test image *vis-à-vis* in a reference template. As mentioned before, a binary correlator approach is adopted to deduce pixel-by-pixel scores of correlations in the 2D-images being compared. Relevant scores decide the underlying contrasting and comparable details in quantifiable terms. Hence, the evaluated scores enable the possibility of finding distinct artefacts in an image as described below.

In all, the pursuits of pattern recognition involve images, which can be specified as spatially discretized set of binary intensities [20][21]. Hence, binary correlators are used as classifiers of patterns (expressed in digital formats) to compare and correlate the underlying image features. A binary correlator in essence, is a classifier that determines, which of a set of classes is most representative of an unknown pattern. In image comparison contexts, it translates to finding the extent of correlation between two image-frames; and, when the images are denoted *via* a matrix of binary variables (1 and 0), the corresponding classification conforms to a binary correlator.

The scope of using such binary correlators in the contexts of image classification is driven by the following considerations: (i) Given the quality of the image expressed in terms of underlying pixel resolution specified in a binary format, optimal use of software and available computer technology can be exercised to extract the information reliably and robustly from the images of interest. (ii) Intricate image details in the local instance can be recognized and classified in binary format while detecting abnormalities (such as, tumours in medical images) situated in a complex ambient of anatomical features and physiological states. (iii) Binary-formated images permit ease in computation and fastness of information extraction from the images on real-time basis as viably needed in clinical applications and medical decisions; and lastly, (iv) known analytical and computational methods can lucidly support analyses of images in binary pixel formats. The steps involved in adopting a binary correlation in image analysis can be outlined as follows: Once the test- and template-images are constructed in binary formats, they can be "compared" to assess the unique features between them (Figure 3). That is, in binary sequence formats, the test-image and the template can be compared on row-to-row and/or column-to-column basis. There are a number of relevant techniques in vogue to perform such correlations and metrics are specified thereof to yield measures on the estimates of the comparison made. For example, use of following metrics are fairly known and cited exemplars in binary data comparison efforts:

- Hopfield net based binary value [22]
- Hamming net based measure [23]
- Haralick parameters [24][25]
- Distance/divergence measures, such as Kullback-Leibler measures [26]
- Needleman-Wunsch (NW) and/or Smith-Waterman (SW) algorithms [3][4]

In the present study, evaluation of relevant cross-correlation scores is done *via* Hamming distance algorithm [23] applied on row-to-row (and column-to-column) of binary entries in the pixels across the matrices developed for the test image and the template (Figure 3).

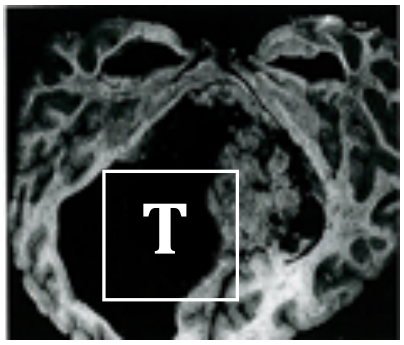


Figure 7: A typical medical-image in analog format. (It refers to a brain-image complex with a tumor spot, marked as, T)

Now, the simulated results obtained in the present study are considered. As mentioned earlier, real-world medical images are in general, complex with local features of fuzzy and/or distorted details; that is, they are not very distinctly discretized as shown in Figure 7. Invariably a gradation of black-to-grey-to-white coloration can be seen diffused across such images, which can be specified only in terms of varying gray level attributes.

With reference to such medical-image contexts, it is first necessary to "locate" the presence of any distinct features in an image. That is, in an analog image having a diffused pattern of coloration, relevant pixel map (with 0 or 1 entries), the associated characteristics of local features (such as tumors, for example marked as **T** in Figure 7) can be considered as unique 'clusters' of pixels/binary numbers; and, the underlying analysis involves ascertaining the location (coordinates) of such 'clusters' and evaluating their characteristic feature map. That is, location of the centroid of the feature-cluster and characteristics of the surroundings having diffused artefacts (fuzzy and/or distorted) are first elucidated.

For example, considering the brain-image (of Figure 7) adopted here for simulation, has a width of about 120 pixel-locations along the horizontal direction; and, there are 60-90, pixel-locations exist from right-to-left; and, they mark approximately the column-wise horizontal dispositions of the tumor site (labeled subspace). Similarly, a total of about 100 pixel-locations map the vertical height of the image; and, top-down pixel locations 40-80 mark approximately the row-wise vertical dispositions of the tumor site (labeled subspace).

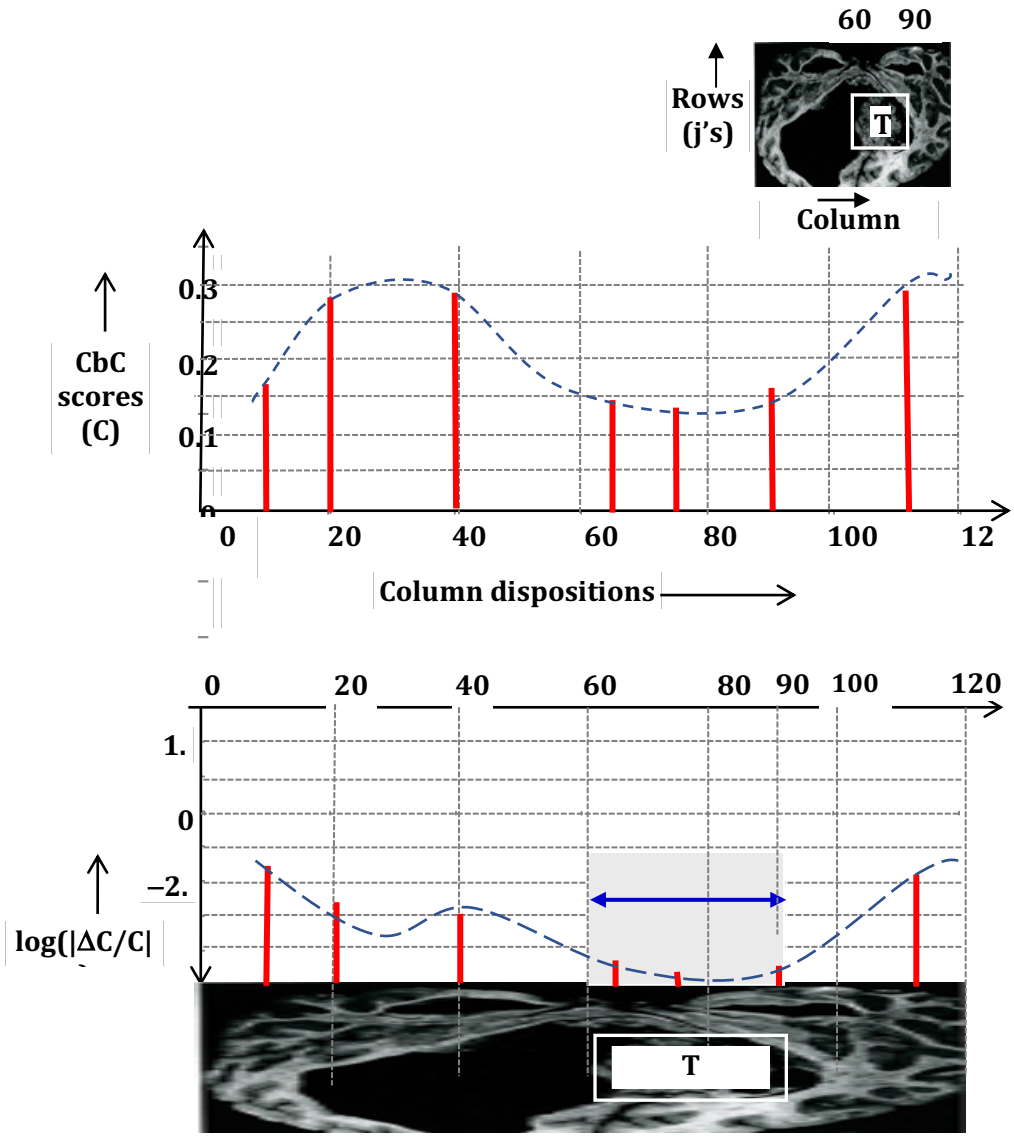


Figure 8a: Computed correlation-scores plotted against pixel dispositions: Column-by-column scores (CbC: C) and corresponding log(|ΔC/C|) values estimated across the entire width of row-wise pixel dispositions

In Figure 8a, the correlation scores obtained *via* row-by-row comparison of the brain image (of Figure 7) *versus* the template image are plotted against the disposition of column pixels. These scores are denoted as, C: CbC. Likewise, the scores obtained *via* column-by-column comparison of the brain image (of Figure 7) *versus* the template image are plotted against the disposition of row pixels in Figure 8b and these scores are indicated as, R: RbR. In both Figures 8a and 8b, the raw scores C and R are also converted to differential log-scales, namely log(|ΔC/C|) and log(|ΔR/R|) where ΔC and ΔR depict the differential values of: (Raw score – Average score). In such differential scales, the background details (outliers) are filtered out and the desired feature-details are rendered to standout. The discussions on the results of Figures 8a and 8b pertinent to the test medical image of Figure 7 are presented in the next section.

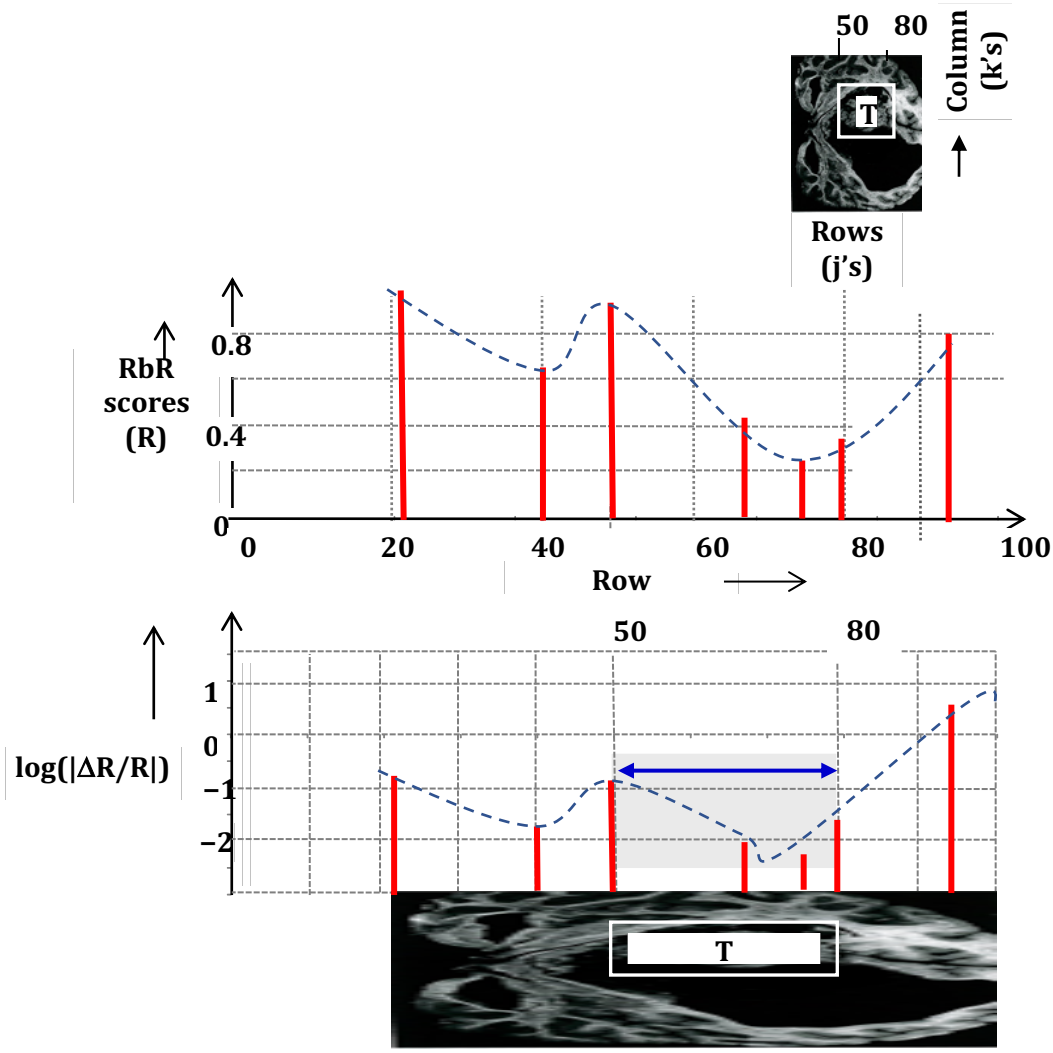


Figure 8b: Computed correlation-scores plotted against pixel dispositions: row-by-by scores (RbR: R) and corresponding log(|DR/R|) values estimated across the entire width of column-wise pixel dispositions

DISCUSSIONS AND CONCLUSIONS

Commensurate with the objectives of this study towards ascertaining the details of a medical-image, relevant image-space presumably has a distorted/fuzzy region, which is mapped as a cluster of pixels having a centroid at (x_o, y_o) as shown in Figure 1. This corrupted/fuzzy (labeled) subspace is regarded as being "noisy" whereas, the uncorrupted sections (unlabeled regions) are presumed to denote genuine/crisp and information-bearing "signal" counterparts. As outlined earlier, the extent of "corruption" or "image-distortion" (relative to a reference/ideal image) associated with the "noisy" subsections in the image at a given cluster of pixel sites centered at (x_o, y_o), can be specified in terms of a 'probability of error' value; and, it is decided by the set of pixel values (1 or 0) estimated around (x_o, y_o). Further, such probability of error values, concurrently lead to specifying the pixel locales to possess a membership value (m). Dominance of probability of error implies the presence of the corrupted sub-space.

In all, the scores deduced at any pixel sites centered at (x_o, y_o) *via* binary correlation techniques implicitly specify the said probability of error, at that site; and, such scores can be used to assess/describe the features of the distorted-image subspaces implicitly. Visualizing and characterizing the locale where a significant artefact (distorted part) in an image such as a tumor is present, the strategy of row-by-row and column-by-column score evaluations *via* correlation algorithms can be performed as illustrated in Figure 3 and detailed in the text.

Using the simulated test FC, the computed details correspond to a test medical image of Figure 7. Its digitized format of 2D pixel array shows that the width of tumor spot (**T**) stretches almost from 60^{th} through 90^{th} (right-to-left) column dispositions of the pixels; and, the height of the tumor spot extends approximately from 50^{th} through 80^{th} top-down row dispositions. Relevantly, the computed, column-by-column correlation scores (C: CbC) and corresponding $\log(|\Delta C/C|)$ values estimated across the entire width of row-wise pixel dispositions are presented in Figure 8a. The results show significantly subdued values across the width of the tumor, wherein the tumor portrays almost a gray-to-white scale (in the test image of Figure 7). However, considering the non-tumor part, stretching approximately from 20^{th} to 60^{th} position, the $\log(|\Delta C/C|)$ score pattern is significantly hiked, corresponding to a near-black scale.

Next, considering the height-wise variations of computed row-by-row, correlation scores (RbR: R) and corresponding $\log(|\Delta R/R|)$ values estimated across the entire width of column-wise pixel dispositions, there are relatively subdued variations of R: RBR and $\log(|\Delta R/R|)$ values across the vertical stretch of the tumor, as can be seen in Figure 8b. Referring the top-layer in the relevant (cropped) matrix as level 20^{th} pixel location, lies between 20^{th} to 50^{th} rows in some peripheral brain material; and, the tumor in question exists approximately between 50^{th} through 80^{th} rows. Further, the coordinate of the centroid of the tumor can be approximately estimated from Figures 8a and 8b, as (60 + 90)/2, (50 + 80)/2. That is, $(x_j, y_k)_i = (x_o, y_o) \approx (75, 65)$. In all, the proposed method enables the possibility of locating and characterizing a distinctly unique feature subspace (labeled region) within an image, using cross-correlation algorithms.

To conclude, the present study demonstrates a promising application of the proposed deep ANN conceived as a fuzzy cognitron for classifying and predicting a labeled pattern being present as an admixture of details in a big data environment. The multilayered deep ANN described thereof conforms to a fuzzy cognitron with an architecture of successively placed set of multiple, paired layers, each containing N neuronal units that are massively interconnected. Each pair of layers is independently trained with an unsupervised learning (USL) schedule. The underlying training and prediction phases are implemented with specifically defined algorithms on sigmoidal squashing in the USL loop; and, the learning rate (α) adopted is obtained by a Hessian matrix (**HD**) approach to yield fast convergence. Simulation details on training a test architecture and evaluating the prediction phase output conform to results *vis-à-vis* fast predictions of labeled data obscurely present in a stochastic mix of unlabeled and labeled patterns addressed as input details at the test ANN. More ever, the study confirms the efficacy of the proposed method and the suggested algorithms. Though there are only seven input details are used in the simulations of the present study with the test FC architecture consisting of three paired layers, (as input, hidden and output layers), the scope of the present

study can be expanded as well with increased number of inputs and architectural details on *ad hoc* basis.

In all, robustness of fuzzy models of ANN architectures warrants high degree of replicated rules applied to evaluate the maps of locally present small disjuncts; and, implementing the analysis of such local models across aggregated details, the required learning algorithm should be a generalization on fragmenting the data on the basis of classifiable/disjunct boundaries. As mentioned earlier, the big data model adopted in the present study refers to considering the presence of two sets of information, namely, a mixed set of fully known and unlabeled domain of sharp image space plus sparsely known, labeled details of local features (fuzzy or otherwise); and, the underlying analyses refer to predicting discriminatively the pattern of desired labeled knowledge sought with minimum error as the outcome. However, such predictions, in general are difficult *vis-a-vis* the associated big data set due to inherent uncertainty in the variety of classes of data stemming from heterogeneous sources with certain details being incomplete disjuncts of veracity in question.

Notwithstanding the complexity of such underlying considerations, a promising effort however, prevails towards designing high performance fuzzy models and algorithms for big data applications in terms of neuromorphic heuristics. Commensurately, this study is offered as a motivated proposal on robust classification schedules conceived towards learning algorithms supported on a class of deep ANN. The test architecture of deep ANN conforms to a fuzzy cognitron. It refers to *the* architecture similar to neocognitron heuristics of Fukushima [15][16]. Relevant network of Figure 4 is a self-organizing multilayered neural network. It is self-organized by "learning without a teacher", and acquires an ability to recognize stimulus patterns based on the any labeled (earmarked) similarity. Its underlying Hebbian learning of a real neural complex conforms to “the synapse from neuron x to neuron y is reinforced when x fires provided that no neuron in the vicinity of y is firing stronger than y”.

In all*,* the *tasks* in *deep neural networking* objectively imply processing a set of raw input data so as to extract required features or the desired/labeled data from it. The extracted details are based on the inherent capability of classification in an arbitrary input-output mapping and specify a predictive classification of the desired data at the output. That is, the ANN is trained to classify the labeled and unlabeled data supplied as the input and spot the labeled pattern as predictive output.

As well known, the ANN has the ability to learn or get trained from experience (or from the existing data). In general, the exhaustively known details adopted for ANN training would conform to a big-data universe wherein the information/pattern to be predicted remains obscured as an admixture of random constituent in the stochastic framework of the large data. The learning exercise imposed on the test ANN as seen earlier, involves adjustment of weight coefficients pertinent to interconnected neuronal units and the adjustment is based on either by capturing the randomness (stochastic aspects) of the stimuli (depicting the input training data) and/or by using information present in a set of tagged (labeled and unlabeled) classification flags present in the input data.

To conclude, the deep ANN conceived as a cognitron possesses self-organization capability with the processed details progressing favorably along deeper layers ahead without having a "teacher" to instruct how the individual neural unit should respond. After repetitive presentations of several stimulus/excitatory patterns, the network becomes self-organized. Further, the receptive fields of the neural computational units/cells become relatively larger in deeper layers with each neuronal unit output layer integrating the information from whole parts of the previous layer and selectively responds to a specific stimulus pattern or a feature.

The proposed approach of FC includes necessary changes in the algorithm so as to accommodate overlapping image features (with imprecise boundaries) normally observed in medical images having artifacts of subspaces. In the present study, the ways of including such fuzzy/distortion considerations refer to resorting to ANN strategies having a suitable architecture that takes digital (binary) inputs and yields details on the required image features at its output. In general, any strategy adopted in image analysis suites would require extensively complex ANN architectures (viewed in terms of supporting large number of inputs and provisioning several counts of layers).

References

1. DeGroff, D., Neelakanta, P. S., A novel deep learning ANN supported on Langevin-Neelakanta machine. Transactions on Machine Learning and Artificial Intelligence, 2022, 10(4), 27-45.

2. DeGroff, D., Neelakanta, P., Forecasting and surveillance of Covid-19 pandemic: A case study using Artificial neural network. Journal of Environmental Science, Computer Science and Engineering & Technology, 2021, Sec. B,10(3), 150-164.

3. Neelakanta, P. S., Pappusetty, D., Bioinformatics-inspired algorithms for 2D-image analysis- application to synthetic and medical images. Part I: Images in rectangular format. International Journal of Biomedical & Clinical Engineering, 2012, 1(1), 14-38.

4. Neelakanta, P. S., Bertot, E. M., Pappusetty, D., Bioinformatics-inspired algorithms for 2D-image analysis-application to synthetic and medical images. Part II: Images in rectangular format. International Journal of Biomedical & Clinical Engineering, 2012, 1(1), 49-58.

5. S. Haykin, S., Moher, M., Communication Systems, 2009, John Wiley & Sons Inc., Hoboken, NJ: USA.

6. Neelakanta, P. S., Information Theoretic Aspects of Neural Networks. 1999, CRC Press, Inc., Boca Raton, Fl: USA.

7. Neelakanta, P. S., DeGroff, D., Neural Network Modeling: Statistical Mechanics and Cybernetic Perspectives. 1994, CRC Press, Inc., Boca Raton, Fl: USA.

8. Neelakanta, P. S., Sharmistha, C., Pavlovic, M., Pandya, A., DeGroff, D., Fuzzy splicing precursor m-RNA sequences: Prediction of aberrant splice-junction in viral DNA context Journal of Biomedical Science and Engineering, 2011, 4, 270-279.

9. Arredondo, T. V., Neelakanta, P. S., De Groff, D., Fuzzy attributes of a DNA complex: Development of a fuzzy inference engine for codon-"junk" codon delineation, Artificial Intelligence in Medicine, 2005, 35, 87-105.

10. Jang, J. -S. R., Sun, C. -T., Mizutani, E., Neuro-fuzzy and Soft Computing, 1997, Springer Verlag., New Jersey: USA.

11. Neelakanta, P. S., Abusalah, S. T., De Groff, D., Park, J. C., Fuzzy nonlinear activity and dynamics of fuzzy uncertainty in the neural complex. Neurocomputing, 1998, 20, 123-153.

12. Chi, Z., Tan, H., Pham, T., Fuzzy Algorithms with Applications to Image Processing and Pattern Recognition. 1996, World Scientific, Singapore.

13. Matzner, T., An algorithm looking at an image simply sees rows of pixels. Nothing else. Humboldt Kosmos, 2022, 114, 15-16.

14. Gu, J., et al., Recent advances in convolutional neural networks. Pattern Recognition. 2018, 77, 354-377.

15. Fukushima, K., Cognitron: A self-organizing multilayered neural network. Biological Cybernetics, 1975, 20, 121-136.

16. Fukushima, K., Neocognitron: A self-organizing neural network model for a mechanism of pattern recognition unaffected by shift in position. 1980, Biological Cybernetics, 36,193-202.

17. Efron, B., Bootstrap methods: Another look at the jackknife. Annals of Statistics. 1979, 7(1), 1-26.

18. Scherzer, O., Mathematical Models for Registration and Applications to Medical Imaging, 2006, Springer-Verlag Berlin-Heidelberg, Germany.

19. Luo, D., Pattern Recognition and Image Processing, 1998, Horwood Publishing Ltd., Chichester, UK.

20. Shalkoff, R. J., Digital Image Processing and Computer Vision, 1988, John Wiley & Sons, New York, NY: USA.

21. Shalkoff, R. J., Pattern Recognition: Statistical, Structural and Neural Approaches, 1992 John Wiley & Sons, New York, NY: USA.

22. Lippmann, R. P., An introduction to the computing with neural networks, 1987, IEEE ASAP Magazine, 4, 4-22.

23. Gallager, R. G., Information Theory and Reliable Commnication, 1968, John Wiley & Sons New York, NY: USA.

24. Haralick, R. M., Shanmugam, K., Dinstein, I., Textural features for image classification, 1973, IEEE Transaction on Systems, Man, and Cybernetics, SMC-3 (6), 610-621.

25. Kalpana, R., Muttan, S., Kumarasamy, N., Virus infection on brain white matter: Statistical analysis of DT MRI scans. 2011, International Journal of Bioinformatics Research and Applications, 7(3), 273 – 286.

26. Kailath, T., The divergence and Bhattacharyya distance measures in signal selection, 1967 IEEE Transactions on Communication Technology, COM-15 (1), 52-60.